

Real-time imaging of DNA loop extrusion by condensin

Mahipal Ganji,¹ Indra A. Shaltiel,^{2*} Shveta Bisht,^{2*} Eugene Kim,¹ Ana Kalichava,¹

Christian H. Haering,^{2†} Cees Dekker^{1†}

¹Department of Bionanoscience, Kavli Institute of Nanoscience Delft, Delft University of Technology, Delft, Netherlands.

²Cell Biology and Biophysics Unit, Structural and Computational Biology Unit, European Molecular Biology Laboratory (EMBL), Heidelberg, Germany.

*These authors contributed equally to this work.

†Corresponding authors. Email: christian.haering@embl.de; c.dekker@tudelft.nl

This is the author's version of the work. It is posted here by permission of the AAAS for personal use, not for redistribution. The definitive version was published in Science 360(6384):102-105, doi: 10.1126/science.aar7831

It has been hypothesized that Structural Maintenance of Chromosomes (SMC) protein complexes such as condensin and cohesin spatially organize chromosomes by extruding DNA into large loops. Here, we provide unambiguous evidence for loop extrusion by directly visualizing the formation and processive extension of DNA loops by yeast condensin in real-time. We find that a single condensin complex is able to extrude tens of kilobase pairs of DNA at a force-dependent speed of up to 1,500 base pairs per second, using the energy of ATP hydrolysis. Condensin-induced loop extrusion is strictly asymmetric, which demonstrates that condensin anchors onto DNA and reels it in from only one side. Active DNA loop extrusion by SMC complexes may provide the universal unifying principle for genome organization.

The spatial organization of chromosomes is of paramount importance to cell biology. Members of the SMC family of protein complexes, including condensin, cohesin, and the Smc5/6 complex, play vital roles in restructuring genomes during the cellular life cycle (1-3). The principles by which SMC complexes achieve these fundamental tasks are still incompletely understood. Models based on random cross-linking of DNA by pairwise interactions or conformational changes in the DNA superhelicity have been proposed (4, 5). An alternative hypothesis suggested that SMC protein complexes bind to small loops in the genome to then processively enlarge them (6). More recently, the idea emerged that condensin can start and subsequently extrude DNA loops, which would elegantly explain how condensin mediates the formation of mitotic chromosomes structures

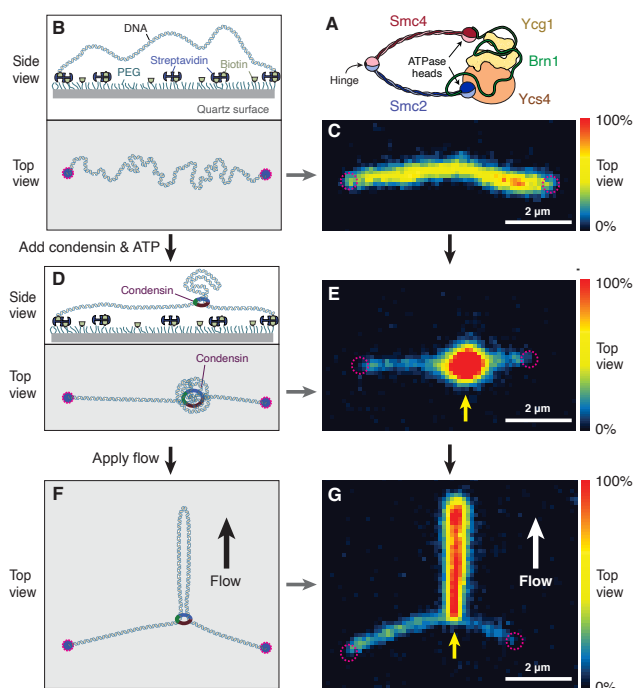


Fig. 1: Single-molecule assay for the visualization of condensin-mediated DNA looping. (A) Cartoon representation of the *S. cerevisiae* condensin complex. (B) Side and top view schematics of DNA that is doubly tethered to a polyethylene glycol (PEG)-passivated quartz surface via streptavidin-biotin linkage. (C) Snap-shot of a double-tethered λ -DNA molecule (100 ms exposure) visualized by Sytox Orange (SxO) staining. Note the homogeneous fluorescence intensity distribution along the DNA. Dashed magenta circles indicate the surface attachment sites of the DNA. (D) Side and top view diagrams showing DNA loop formation on double-tethered DNA by condensin. (E) Snap-shot of condensin-mediated DNA loop formation at one spot (indicated by the yellow arrow) along a SxO-stained DNA molecule. (F) Strategy to visualize DNA loops. Application of flow perpendicular to the axis of the immobilized DNA extends the loop within the imaging plane. (G) Snap-shot of an extended DNA loop that is stretched out by flow (white arrow) perpendicular to the DNA, as illustrated in (F).

observed in electron micrographs and deduced from Hi-C experiments (7, 8). Indeed, polymer simulations showed that loop extrusion can, in principle, result in the efficient disentanglement and compaction of chromatin fibers (9–11). The recent discovery that condensin exhibits DNA translocase activity (12) was consistent with, but did not provide conclusive evidence for (13), DNA loop extrusion.

In this Report, we visualize the formation of DNA loops by the *Saccharomyces cerevisiae* condensin complex in real time (Fig. 1A). We tethered both ends of a double-stranded 48.5-kilobase pair (kbp) λ -DNA molecule to a passivated surface (14, 15), using flow to adjust the DNA end-to-end length to a distance much shorter than its contour length (Fig. 1B). We then imaged DNA after staining with Sytox Orange (SxO; Fig. 1C and movie S1). Upon flushing in 1 nM of condensin (12) and 5 mM of adenosine triphosphate (ATP), we observed the accumulation of fluorescence density at one spot along the length of the DNA (Fig. 1, D and E, fig. S1, and movie S2). This finding shows that condensin induces local compaction of DNA.

To visualize the compacted DNA structures in the imaging plane of the microscope, we applied flow at a large angle with respect to the double-tethered DNA. This revealed that the bright spots were made up of extended pieces of DNA, consistent with single large DNA loops (Fig. 1, F and G, fig. S2, and movie S3). Importantly, we observed no DNA loop formation by wild-type condensin in the absence of either ATP or Mg^{2+} , when we replaced ATP by the non-hydrolyzable analogues ATP γ S or AMPPNP, or when we used a mutant condensin that is unable to bind ATP. Condensin hence creates DNA loops in a strictly ATP-hydrolysis-dependent manner, either by gradually extruding DNA or by randomly grabbing and linking two DNA loci.

To distinguish between these two possibilities, we monitored the looping process by real-time imaging of the DNA while applying constant flow. This revealed the gradual appearance of an initially weak increase in fluorescence intensity at a local spot that grew into an extended loop over time (Fig. 2A, fig. S3, and movies S4 and S5), providing direct visual evidence of loop extrusion and ruling out the random cross-linking model. The extruded loops were in general stable (fig. S4), but occasionally disrupted spontaneously in a single step (Fig. 2A and movie S6). Such a single-step disruption suggests that the DNA loop had been extruded by a single condensin unit that spontaneously let go of the loop, instead of a multi-step relaxation of the loop due to multiple units.

Higher-temporal-resolution imaging allowed us to resolve the two individual DNA strands in the extruded loop in

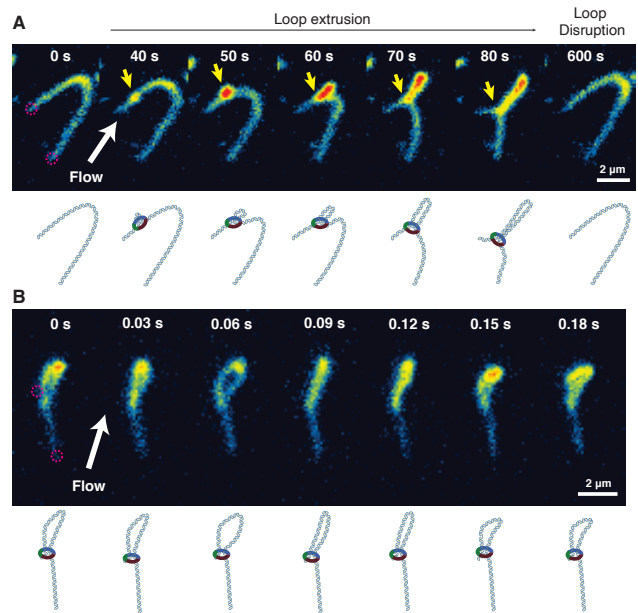


Fig. 2: Real-time imaging of DNA loop extrusion by condensin. (A) Series of snap-shots showing DNA loop extrusion intermediates created by condensin on a SxO-stained double-tethered λ -DNA (Movie S3). A constant flow at a large angle to the DNA axis (white arrow) maintains the DNA in the imaging plane and stretches the extruded loop. A yellow arrow indicates the position of the loop base. At ~40 s, a small loop appears that grows over time until ~80 s, consistent with the loop extrusion model. A random linkage model would instead have predicted the sudden appearance of a loop that would have remained stable in size over time. After ~600 s, the loop suddenly disrupted. Schematic diagrams under each snap-shot are for visual guidance. (B) High time-resolution imaging reveals the splitting of the two DNA strands in the extruded loop in adjacent time frames.

consecutive time frames, which showed that condensin had extruded an actual loop rather than an intertwined, supercoiled, or otherwise connected structure (Fig. 2B, fig. S5, and movie S7).

To quantify the kinetics of loop extrusion, we returned to imaging in the absence of flow. We constructed kymographs from movies where the loop first nucleated as a single weak fluorescent spot that subsequently expanded in size over time (Fig. 3, A and B, and movie S8). We divided each line of the kymograph into the regions outside the loop (I and III) and the DNA loop region itself (II) and calculated, for every frame, the DNA lengths from the fluorescence intensity in each region (Fig. 3C and fig. S6A). This revealed the extrusion of sizeable amounts of DNA into the loop (region II), ranging from 5 kbp to 40 kbp (the upper limit of our assay) before reaching a plateau (fig. S6, B and C). Simultaneously, the DNA content of one of the two outside regions (III) decreased by the same amount, whereas the DNA content of the other outside region (I), surprisingly, did not change at all during the loop-extrusion process (Fig. 3, D to F). This result was consistent in all loop extrusion events that we analyzed quantitatively (N=36; fig. S6, B to D) and strikingly demonstrates that the loop extrusion process is asymmetric – a finding that is in stark contrast to theoretical loop-

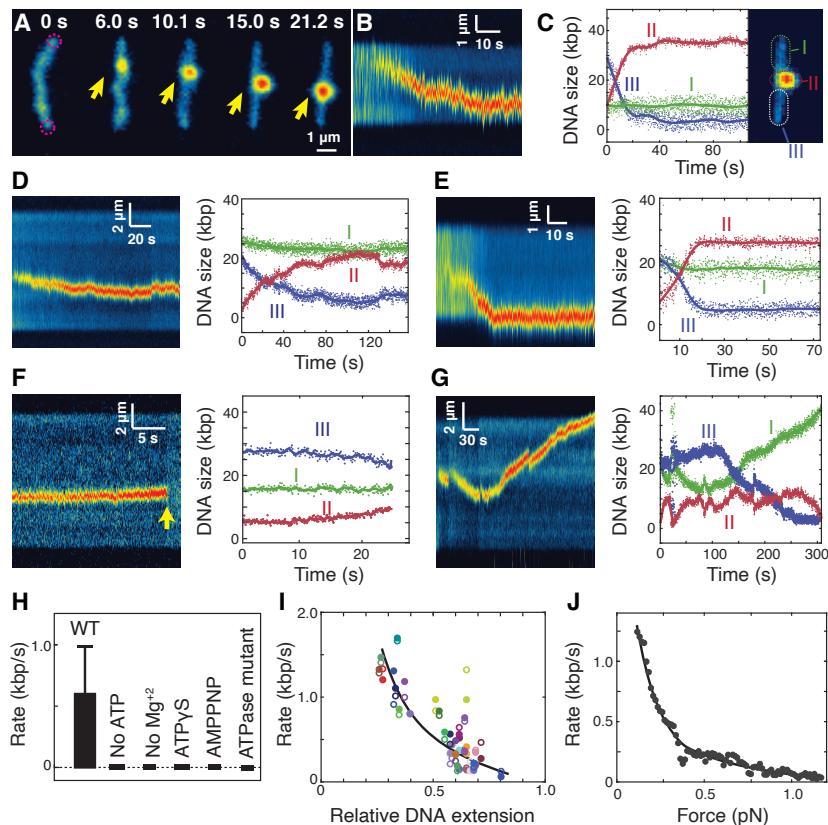


Fig. 3: Loop extrusion is asymmetric and depends on ATP hydrolysis. (A) Snap-shots showing the gradual extension of a DNA loop (yellow arrow) on a double-tethered λ -DNA molecule. (B) Kymograph of SxO fluorescence intensities shown in (A). (C) DNA lengths calculated from the integrated fluorescence intensities and the known 48.5-kbp length of the λ -DNA in the kymograph of panel (B) for regions outside the loop (I and III) and the loop region itself (II). (D–F) Fluorescence kymographs and intensity plots of a more stretched DNA molecule (end-to-end distance 9.1 μm) where the DNA loop stalls midway (D), of a DNA molecule where loop extrusion starts in the center and continues until reaching the physical barrier at attachment site (E), and of a loop-extrusion event that abruptly disrupts in a single step. (G) Kymograph and intensity plot for loop extrusion by a safety-belt condensin mutant complex, which displays dynamic changes of all three DNA regions and of the loop position. (H) Average loop extrusion rates (mean \pm SD) under various conditions. (I) Rate of loop extrusion plotted versus the relative DNA extension in relation to its 20- μm contour length. Filled circles are calculated from region II, open circles from region III, the line serves as a visual guide. (J) Rate of loop extrusion plotted versus the force exerted within the DNA due to increased DNA stretching upon increase of the loop size. The line serves as a visual guide.

extrusion models that have so far been based on two linked motor domains that translocate along the DNA in opposite directions, thereby reeling in DNA symmetrically from both sides (9–11).

The asymmetry can be explained if one site in the condensin complex remains stably anchored to the DNA while its motor site translocates along the same DNA. A candidate for such a DNA anchor site is the charged groove formed by the Ycg1 HEAT-repeat and Brn1 kleisin subunits, which entraps DNA by a safety-belt mechanism (16). When we repeated the loop-extrusion experiments with a mutant condensin that is unable to fasten the safety belt, the extruded loops no longer remained stable over time, but instead changed size and frequently moved its position (Fig. 3G and fig. S7), resulting in a DNA decrease in one and increase in the other outside region (compare the green curves in fig. 3, C to G). Furthermore, when we increased the NaCl and Mg^{2+} concentrations of the buffer, we observed unidirectional motion of the extruded loop (fig. S8). The weakening of a stable anchoring point in both experiments is consistent with slippage of DNA through the safety belt. The latter finding also explains the observation of condensin translocation on DNA under the same buffer conditions (12).

We can estimate the speed of DNA loop extrusion from the slopes of the initial linear part of the extrusion curves, which yields an average rate of 0.6 kbp/s. As expected, this rate depends on the concentration of ATP (fig. S9) and

ATP hydrolysis by condensin (Fig. 3H). Correlation with the end-to-end lengths of individual DNA molecules showed that the speed and efficiency of loop extrusion strongly depended on the relative extension of the DNA, with rates of up to ~ 1.5 kbp/s and $>80\%$ of all DNA molecules displaying loop extrusion at lower DNA extensions (Fig. 3I and fig. S10). Although a direct comparison with Hi-C experiments is impeded by the complexity of chromosomes in cells, it is nevertheless remarkable that condensation rates calculated by this method for condensin II (0.1–0.2 kbp/s) (17) or a bacterial SMC complex (0.9 kbp/s) (18) are in the same order of magnitude. We note that our assay provides a direct measurement of the condensation rate by individual condensin molecules, since it avoids any discussions about roadblocks, multiple condensin units working in series or in parallel at different positions on the DNA, etc.

The dependence of the extrusion rate on the DNA end-to-end length can be understood as a force dependence: As the loop is extruded, the amount of DNA between the two attachment points (excluding the loop) decreases correspondingly, thus continuously increasing the tension within the DNA (19) (to 1.2 ± 0.5 pN; $N=23$; see Methods) until the loop-extrusion process stalls (see, for example, fig. 3D). We used the known force-extension relation for DNA to plot the loop extrusion rate versus force, which revealed a steep dependence on force (Fig. 3J and fig. S11). This very strong force dependence, where the loop

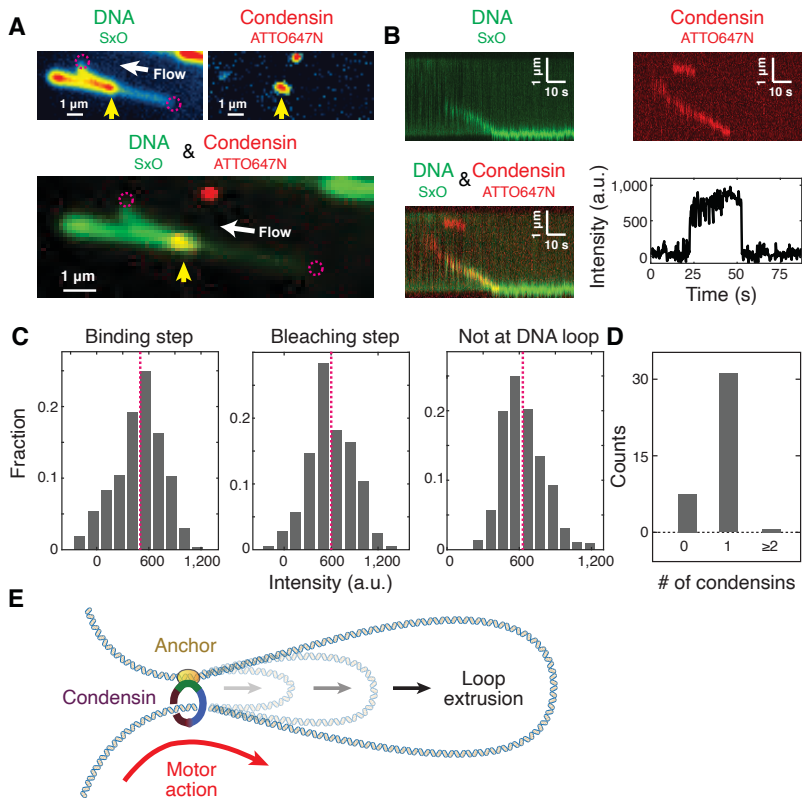


Fig. 4: Loop extrusion is induced by a single condensin complex. (A) Images of the same field of view of SxO-stained DNA (top left), ATTO647N-labeled condensin (top right) and their merge (bottom) reveal condensin at the stem of an extruded DNA loop (yellow arrow). Images are integrated over 2 s of a movie. (B) Kymographs of SxO-stained DNA (top left), ATTO647N-condensin (top right) and their merge (bottom left) of a real-time movie of DNA loop extrusion. The corresponding ATTO647N fluorescence time trace (bottom right) shows single-step binding and single-step photobleaching events of the DNA-bound condensin. (C) Fluorescence intensity distributions for condensin binding events that led to DNA-loop extrusion (left), condensin bleaching in such events (middle), and binding events that did not lead to loop extrusion (right) measured under similar optical conditions. (D) Histogram of the number of condensin complexes that show loop extrusion activity as counted from the fluorescence steps. (E) Model for DNA loop extrusion by condensin. One strand of DNA is anchored by the kleisin and HEAT-repeat subunits (yellow-orange) of the condensin complex, which extrudes a loop of DNA.

extrusion rate drops significantly near 0.4 pN, is consistent with previous magnetic tweezer experiments (20–22), which also reported condensation rates that match the loop extrusion rates that we measured at similar forces (Fig. 3J). Together, these findings show that condensin is a fast, yet weak loop-extruding motor that rapidly stalls against a modest force applied to the DNA.

We measured an ATP hydrolysis rate of ~ 2 molecules per second for condensin in the presence of DNA (fig. S12A). Notably, such a bulk estimate only provides a lower limit of the ATPase activity of condensin complexes in the active loop-extrusion process, since non-DNA-bound condensin molecules and complexes that have stalled on the DNA are included in these assays. If we nevertheless assume, for the sake of argument, that condensin hydrolyzes 2 ATP for extruding ~ 110 nm (~ 0.6 kbp) of the folded DNA every second, it would take steps in the order of the 50-nm size of a single condensin complex. Scenarios that explain such large steps must be very different from those for conventional DNA motor proteins that move in single base pair increments (23). Models likely need to involve the flexibility of DNA, which allows that, for low forces, condensin can reach nearby spots on the folded DNA to occasionally capture and extrude much longer stretches of DNA than the condensin size itself (12, 24, 25). This would be consistent with the very strong force dependence of the extrusion rate that we observe.

Finally, we labeled purified condensin holocomplexes with a single ATTO647N fluorophore (fig. S12) and co-imaged them with SxO-labeled DNA in a Highly Inclined and Laminated Optical (HILO) sheet mode (26). As expected, ATTO647N-condensin frequently localized to the stem of the extruded DNA loop (Fig. 4A, fig. S13 and movies S9 and S10). Using real-time monitoring, we consistently observed DNA binding of condensin in a single-step appearance, followed by DNA loop extrusion, and finally single-step bleaching (Fig. 4B, figs. S14 and S15; $N=20$). This sequence of events demonstrates that the DNA loop was extruded by a single condensin complex. Kymographs also revealed another class of condensin binding and unbinding events with a short dwell-time that did not lead to DNA loop extrusion (fig. S16A). These were the only DNA-binding events in the absence of ATP (fig. S16B). Furthermore, we observed events where a DNA loop disrupted, while condensin stayed bound to the DNA and later started to extrude a new DNA loop (fig. S14, D and E) – showing that in the process of loop disruption, condensin spontaneously releases the extruded loop rather than dissociates from the DNA.

Quantification of the ATTO647N-condensin intensity provided further evidence that it is a single condensin complex that locates to the stem of the DNA loop: We compared the fluorescence intensity for three cases, (i) condensin binding events that led to DNA loop extrusion, (ii) condensin bleaching events, and (iii) temporary binding events that did not lead to loop extrusion. All three cases revealed the same change in intensity (Fig. 4C), showing that a single condensin complex localizes to the stem of the DNA loop (Fig. 4D). If two condensin

complexes would assemble at the loop stem, one would instead have expected a bimodal intensity distribution with two peaks of similar height for single- and double-labeled condensin dimers (based on a 60–85% labeling efficiency, see Methods). Instead, we observed no two-step bleaching events, a majority fraction (33/40) of single-step bleaching events, and a small fraction of DNA molecules (7/40) that showed DNA loop extrusion without any visible fluorescence (fig. S17), as expected for a labeling efficiency of 82%.

Although SMC complexes are vital for chromosome organization in all domains of life, the molecular basis for their action so far remained largely speculative. Our experiments unambiguously demonstrate that condensin exhibits DNA loop-extrusion activity. Our real-time single-molecule dual-color movies of condensin and DNA reveal that loops are extruded by a single condensin complex at the stem of the loop in a manner that is ATP hydrolysis-dependent, strictly asymmetric, and highly sensitive to forces applied to the DNA. These properties can be explained by a model (Fig. 4E) where condensin makes stable contact with DNA at a binding site and then reels in DNA from only one side. The visual proof that condensin is a loop-extruding enzyme reveals the key principle that underlies the organization of genome architecture by condensin and most likely all other SMC protein complexes.

Acknowledgments:

We thank M. Kschonsak for providing the safety-belt mutant condensin complex, J. Kerssemakers and J. van der Torre for technical support, and J. Eeftens, A. Katan, J.-K. Ryu, and E. van der Sluis for discussions. **Funding:** This work was supported by the ERC grants SynDiv 669598 and CondStruct 681365, the Netherlands Organization for Scientific Research (NWO/OCW) as part of the Frontiers of Nanoscience program and a Rubicon Grant, and the European Molecular Biology Laboratory (EMBL). **Author contributions:** M. G. and C. D. designed the single-molecule visualization assay, M. G., E. K., and A. K. performed the imaging experiments, I. A. S. and S. B. developed condensin fluorescence labeling strategies and purified protein complexes, I. A. S. performed ATPase assays, C. D. and C. H. H. supervised the work, M. G., C. H. H., and C. D. wrote the manuscript with input from all authors. **Competing interests:** All authors declare that they have no competing interests. **Data and materials availability:** Original imaging data and protein expression constructs are available upon request.

References and Notes:

1. L. Aragon, E. Martinez-Perez, M. Merkschlager, Condensin, cohesin and the control of chromatin states. *Current Opinion in Genetics & Development* **23**, 204-211 (2013).
2. F. Uhlmann, SMC complexes: from DNA to chromosomes. *Nature Reviews Molecular Cell Biology* **17**, 399 (2016).
3. K. Jeppsson, T. Kanno, K. Shirahige, C. Sjogren, The maintenance of chromosome structure: positioning and functioning of SMC complexes. *Nature Reviews Molecular Cell biology* **15**, 601-614 (2014).
4. T. Hirano, Condensin-Based Chromosome Organization from Bacteria to Vertebrates. *Cell* **164**, 847-857 (2012).
5. R. Thadani, F. Uhlmann, S. Heeger, Condensin, Chromatin Crossbarring and Chromosome Condensation. *Current Biology* **22**, 1012-1021 (2012).
6. K. Nasmyth, Disseminating the Genome: Joining, Resolving, and Separating Sister Chromatids During Mitosis and Meiosis. *Annual Review of Genetics* **35**, 673-745 (2001).
7. J. R. Paulson, U. K. Laemmli, The structure of histone-depleted metaphase chromosomes. *Cell* **12**, 817-828 (1977).
8. N. Naumova *et al.*, Organization of the Mitotic Chromosome. *Science* **342**, 948-953 (2013).
9. A. Goloborodko, M. V. Imakaev, J. F. Marko, L. Mirny, Compaction and segregation of sister chromatids via active loop extrusion. *eLife* **5**, e14864 (2016).
10. E. Alipour, J. F. Marko, Self-organization of domain structures by DNA-loop-extruding enzymes. *Nucleic Acids Research* **40**, 11202-11212 (2012).
11. A. Goloborodko, John F. Marko, Leonid A. Mirny, Chromosome Compaction by Active Loop Extrusion. *Biophysical Journal* **110**, 2162-2168 (2016).
12. T. Terakawa *et al.*, The condensin complex is a mechanochemical motor that translocates along DNA. *Science* **358**, 672-676 (2017).
13. K. Nasmyth, How are DNAs woven into chromosomes? *Science* **358**, 589-590 (2017).
14. M. Ganji, S. H. Kim, J. van der Torre, E. Abbondanzieri, C. Dekker, Intercalation-Based Single-Molecule Fluorescence Assay To Study DNA Supercoil Dynamics. *Nano letters* **16**, 4699-4707 (2016).
15. S. H. Kim, M. Ganji, J. v. d. Torre, E. Abbondanzieri, C. Dekker, DNA sequence encodes the position of DNA supercoils. *bioRxiv* (2017).
16. M. Kschonsak *et al.*, Structural Basis for a Safety-Belt Mechanism That Anchors Condensin to Chromosomes. *Cell* **171**, 588-600 (2016).
17. J. H. Gibcus *et al.*, A pathway for mitotic chromosome formation. *Science*, eaa06135 (2018).
18. X. Wang, H. B. Brandão, T. B. K. Le, M. T. Laub, D. Z. Rudner, Bacillus subtilis SMC complexes juxtapose chromosome arms as they travel from origin to terminus. *Science* **355**, 524-527 (2017).
19. C. Bustamante, S. B. Smith, J. Liphardt, D. Smith, Single-molecule studies of DNA mechanics. *Current Opinion in Structural Biology* **10**, 279-285 (2000).
20. J. M. Eeftens *et al.*, Real-time detection of condensin-driven DNA compaction reveals a multistep binding mechanism. *The EMBO journal* **36**, 3448-3457 (2017).
21. J. Eeftens, C. Dekker, Catching DNA with hoops—biophysical approaches to clarify the mechanism of SMC proteins. *Nature Structural Molecular Biology* **24**, 1012-1020 (2017).
22. T. R. Strick, T. Kawaguchi, T. Hirano, Real-Time Detection of Single-Molecule DNA Compaction by Condensin I. *Current Biology* **14**, 874-880 (2004).
23. W. Yang, Lessons learned from UvrD helicase: mechanism for directional movement. *Annual review of biophysics* **39**, 367-385 (2010).

24. J. Lawrimore, B. Friedman, A. Doshi, K. Bloom, RotoStep: A Chromosome Dynamics Simulator Reveals Mechanisms of Loop Extrusion. *Cold Spring Harbor Symposia on Quantitative Biology* **033696**, (2017).
25. M.-L. Diebold-Durand *et al.*, Structure of Full-Length SMC and Rearrangements Required for Chromosome Organization. *Molecular Cell* **67**, 334-347 (2017).
26. M. Tokunaga, N. Imamoto, K. Sakata-Sogawa, Highly inclined thin illumination enables clear single-molecule imaging in cells. *Nature Methods* **5**, 159-161 (2008).
27. J. Yin, A. J. Lin, D. E. Golan, C. T. Walsh, Site-specific protein labeling by Sfp phosphopantetheinyl transferase. *Nature protocols* **1**, 280-205 (2006).
28. J. Yin *et al.*, Genetically encoded short peptide tag for versatile protein labeling by Sfp phosphopantetheinyl transferase. *Proceedings of the National Academy of Sciences of the United States of America* **102**, 15815-15820 (2005).

Materials and Methods

Preparation of biotin-labeled λ -DNA

The single-stranded DNA ends of lambda phage DNA (λ -DNA; D1521, Promega) were filled with DNA polymerase I large fragment (M0210, New England Biolabs), which lacks the exonuclease activity, in the presence of dTTP, dCTP, dGTP, and biotin-14-dATP (19524016, Invitrogen). The biotin-labelled DNA was then purified from excess nucleotides and polymerase using a PCR clean up kit (20021, Qiagen). This preparation produced DNA molecules of which the majority contained biotin moieties on both ends, as evidenced by the large fraction of DNA molecules that assembled as double tethers on the streptavidin-coated surfaces in our assay (fig. S1). Note that molecules that did not incorporate biotin do not bind to the surface of the flow-cell, whereas molecules with a biotin moiety at only one of the two ends result in single-tethered DNAs that were ignored in the data analysis. The biotin-labelled DNA was stored at -20°C until use.

Condensin holocomplex purification

Pentameric *S. cerevisiae* condensin complexes were purified as reported previously (12). Briefly, *S. cerevisiae* cells were transformed with a pair of 2μ -based high copy plasmids containing *pGAL10-YCS4 pGAL1-YCG1 TRP1* and either *pGAL7-SMC4-StrepII₃* *pGAL10-SMC2 pGAL1-BRN1-His₁₂-HA₃ URA3* (wild-type, strain C4491), *pGAL7-smc4(Q302L)-StrepII₃ pGAL10-smc2(Q147L) pGAL1-BRN1-His₁₂-HA₃ URA3* (Q-loop ATPase mutant, strain C4724), or *pGAL7-SMC4-StrepII₃ pGAL10-SMC2 pGAL1-brn1(M391D, F394D, W402D, W408D)-His₁₂-HA₃ URA3* (safety belt mutant, strain C5037). Overexpression was induced by addition of galactose to 2% in $-\text{Trp } -\text{Ura}$ media. Cell lysates were prepared in buffer A (50 mM TRIS-HCl pH 7.5, 200 mM NaCl, 5% (v/v) glycerol, 5 mM β -mercaptoethanol, 20 mM imidazole) supplemented with $1\times$ cComplete EDTA-free protease inhibitor mix (11873580001, Roche) in a FreezerMill (Spex), cleared by centrifugation, loaded onto a 5-mL HisTrap column (GE Healthcare) and eluted with 220 mM imidazole in buffer A. Eluate fractions were supplemented with 1 mM EDTA, 0.2 mM PMSF and 0.01% Tween-20, incubated overnight with Strep-Tactin Superflow high capacity resin (2-1208-010, IBA), and eluted with buffer B (50 mM TRIS-HCl pH 7.5, 200 mM NaCl, 5% (v/v) glycerol, 1 mM DTT) containing 10 mM desthiobiotin. After concentrating the eluate by ultrafiltration, final purification proceeded by size-exclusion chromatography with a Superose 6 column (GE Healthcare) pre-equilibrated in buffer B containing 1 mM MgCl_2 . Purified protein was snap-frozen and stored at -80°C until use.

ATPase assays

ATP hydrolysis assays were performed essentially as described (12). Reactions were set up in a volume of 10 μL , containing 0.25 μM condensin in 50 mM TRIS-HCl pH 7.5, 50 mM NaCl, 2.5 mM MgCl_2 , 1.25% (v/v) glycerol, 3.75% (w/v) D-glucose and 1 mM DTT. Where indicated, 1 μg λ -DNA (N3011S, New England Biolabs) was included in the reaction. Reactions were initiated by addition of ATP to 5 mM (containing 6.7 nM [α - ^{32}P]ATP) and incubated at room temperature. Every 180 s, for six consecutive time intervals, 1 μL of the reaction was spotted onto PEI cellulose F TLC plates (Merck), which were developed in 0.5 M LiCl and 1 M formic acid, exposed to imaging plates, and analyzed on a Typhoon FLA9500 imager (GE Healthcare).

Fluorescent labeling of purified condensin complexes

A ybbR acceptor peptide sequence (GTDSLEFIASKLA; (27)) was introduced into the overexpression plasmid at the N terminus of Brn1, replacing amino acid residues 13–23 of the original protein. Condensin complexes containing the ybbR tag and cleavage sites for tobacco etch virus (TEV) protease were purified from yeast cells as before (strain C5066 for wild-type). The CoA-ATTO647N substrate for covalent coupling to the Serine hydroxyl group of the ybbR peptide was synthesized as described (28): 50 nmol of ATTO647N-maleimide (AD 647N-41, ATTO-TEC) were incubated at room temperature with 45.5 nmol Coenzyme A sodium salt hydrate (C3144, Sigma) in 0.1 mL of a 50:50 (v/v) mixture of DMSO:100 mM sodium phosphate pH 7.0 (aq; degassed). 15 minutes into the reaction, 100 nmol of tris(2-carboxyethyl)phosphine (646547, Sigma) were included and the reaction was quenched after one hour by addition of dithiothreitol to 330 nmol.

For the subsequent transfer of the ATTO647N-succinimidyl phosphopantetheine thioether moiety, purified condensin complexes (~5 μM) were incubated with a five-fold molar excess of CoA-ATTO647N in buffer B supplemented with 10 mM MgCl_2 and 1.2 μM Sfp phosphopantetheinyl transferase (P9302, New England Biolabs) for 16 hours at 6°C, shielded from light. After ultrafiltration, free dye and Sfp synthase were eliminated by size exclusion chromatography on a Superose 6 Increase column (GE Healthcare) pre-equilibrated in buffer B containing 1 mM MgCl_2 (fig. S12, C to E). Peak fractions were pooled and concentrated by ultrafiltration. Fractions were analyzed by SDS-PAGE (NuPAGE 4-12% Bis-Tris gels, ThermoFisher) and fluorescence was detected on a Typhoon FLA9500 imager (GE Healthcare) with a 635-nm laser and a 665-nm long pass filter.

Labeling efficiency was estimated to be 60-85% based on the absorbance ratio of 280 and 650 nm, using the calculated molar extinction coefficient of the condensin complex at 280 nm ($335,670 \text{ M}^{-1} \text{ cm}^{-1}$), the molar extinction coefficient of the ATTO647N dye at 650 nm ($150,000 \text{ M}^{-1} \text{ cm}^{-1}$), and correcting for the absorption at 280 nm by the dye ($\epsilon_{280 \text{ nm}}/\epsilon_{650 \text{ nm}} = 0.03$).

Double-tethered DNA assay for single-molecule imaging

Microfluidic chambers were prepared using biotin-PEG/PEG-passivated quartz slides and cover slips as described previously (14). The volume of the flow cell was about 20 μL . The chambers were first incubated with 0.1 mg/mL streptavidin in T20 buffer (40 mM TRIS-HCl pH 7.5, 20 mM NaCl, 0.2 mM EDTA) for 1 min. Unbound streptavidin was washed off with 100 μL of T20 buffer. 35 μL of ~1 pM biotin-labelled DNA in T20 buffer was then introduced into the flow cell at a constant speed of 5-20 $\mu\text{L}/\text{min}$. Immediately thereafter, excess DNA was washed off with 100 μL of T20 buffer at the same flow rate. This preparation resulted in a sparse distribution of double-tethered DNA molecules that could be imaged individually. The surface-tethered DNA molecules were stained with 500 nM of Sytox Orange (S11368, ThermoFisher) in imaging buffer (50 mM TRIS-HCl pH 7.5, 50 mM NaCl, 2.5 mM MgCl_2 , 1 mM DTT) and an oxygen scavenging system (5% (w/v) D-dextrose, 2 mM Trolox, 40 $\mu\text{g}/\text{mL}$ glucose oxidase, 17 $\mu\text{g}/\text{mL}$ catalase).

For imaging of SxO-stained DNA only, a 532-nm laser was used in a home-built epifluorescence microscope (14). In the case of dual-color imaging of SxO-stained DNA and

ATTO647N-labelled condensin, 532-nm and 640-nm lasers for SxO and ATTO647N excitation were used in Highly Inclined and Laminated Optical sheet (HILO) microscopy mode (26) with an NA 1.49 CFI APO TIRF 100× oil immersion objective (Nikon). HILO microscopy allowed for imaging SxO-stained λ -DNA and ATTO647N-labeled condensin with a high signal-to-noise ratio, while avoiding high fluorescence background resulting from free-floating labeled condensin molecules. The simultaneous imaging of λ -DNA and condensin was achieved by an alternating excitation scheme.

Image analysis and data processing

Fluorescence images were analysed using custom-built Matlab (Mathworks) software as described previously (14). Fluorescence intensity profiles of DNA molecules exhibiting loop structures were obtained by summing the intensity values from 11 pixels taken across a line perpendicular to the extended DNA in each frame. Background intensity was removed by 2d-median filtering. Subsequently, the intensities were normalized to the maximum value in order to correct for intensity fluctuations (such as bleaching) during the measurements. After obtaining the intensities for all frames, the normalized intensity profiles taken at subsequent time points were concatenated to build an intensity kymograph, such as shown in figure 3, B and D–G.

From the kymographs obtained from individual DNA molecules, the amount of DNA in regions I, II, and III (Fig. 3, C–G) was estimated as following. The position of the maximum fluorescence intensity at the looped DNA was used to determine the position of the loop. As the loop is positioned on top of the extended DNA, integrated intensity around the maximum intensity pixel will contain the intensity of the extended DNA as well. To correct for the extended DNA beneath the loop, the backbone DNA intensity was subtracted. The size of the loop was determined by integrating the intensity from 11 pixels centred at the pixel with maximum intensity. The total intensity of DNA was determined ahead and behind the loop. Using the intensity information, the size of DNA (in kbp) in the loop, ahead, and behind the loop was obtained by normalization with the entire DNA intensity and multiplication by 48.5 kbp, i.e.:

$$DNA \text{ size in loop (bp)} = \frac{(Int_{Loop} * 48,502)}{Total \text{ DNA intensity}}$$

$$DNA \text{ ahead of loop (bp)} = \frac{(Int_{ahead \text{ of loop}} * 48,502)}{Total \text{ DNA intensity}}$$

$$DNA \text{ behind of loop (bp)} = \frac{(Int_{behind \text{ of loop}} * 48,502)}{Total \text{ DNA intensity}}$$

The DNA loop extrusion rate was determined in two ways: First, the rate was obtained from the slope of a simple linear fit to the linear rise in the first 15 seconds of the data shown in figure S6B, region II. The resulting data for the DNA loop extrusion rates are shown in figures 3I and S6D. In a second analysis, the nonlinear change of the loop extrusion rate versus time was considered. To extract the loop-extrusion rate in this regime, the time trace for the growth of DNA loop (for example, red curve in figure 3C) was

smoothed using the Savitzky-Golay method (2nd polynomial order) with a moving window of 100 points. This was followed by taking the first derivative between adjacent points, which yielded the extrusion rate in kbp/s at every time point. The result is a loop-extrusion rate that changes over time (see figure S11 for an example). Note that the rate drops quickly as loop growth proceeds.

For figure 3I, the relative extension of the DNA was obtained by dividing the observed end-to-end length of the DNA molecule by the contour length (20 μm for the full-length λ -DNA after 500 nM SxO intercalation) of the piece of λ -DNA that is not contained in the loop. The DNA loop extrusion rate was then plotted against this relative extension in figure 3I.

For figure 3J, the force acting within the DNA was obtained from the relative extension of the DNA. The relative extension of DNA was converted to force via linear interpolation of the known force-extension curve that was experimentally obtained by single-molecule magnetic tweezer force spectroscopy (14). Note that the force exerted on DNA vs relative extension was independent of SxO concentration (14) and thus the known force-relative extension curve from Ganji and Kim *et al.* could simply be used to read off the forces from the experimental extension data. Figure 3J plots the loop extrusion rate as a function of the applied force thus calculated, for a number of individual molecules (N=23) that all exhibited stalling of the loop extrusion somewhere mid-molecule, i.e. where the DNA loop extrusion was not limited by reaching the end position of the DNA. The plot in figure 3J displays the average of the 23 curves from individual molecules (cf. figure S11D) for which the data are averaged across the common range of forces with a bin size of 0.012 pN.

We used a custom single-particle tracking algorithm written in MATLAB to track the ATTO647N-labeled condensin molecule on DNA in HILO microscopy. Using the tracked fluorescence intensity, we constructed intensity-time traces as shown in figures 4B, bottom right, and S15. The intensity histograms in figure 4C (left and middle) were constructed from all the obtained time traces that showed single-step binding, DNA loop extrusion, and single-step photobleaching. From the time traces that showed photobleaching, ATTO647N fluorescence intensity for 10 time points at the binding step (left) and 10 time points before photobleaching step (middle) was plotted (Fig. 4C, left and middle). We also observed condensin binding to DNA and dissociating without any loop extrusion activity (see, for example, the appearance of an ATTO647N signal in the kymographs in figures 4B, right, and S14, A, C, and E). We analysed the intensity of such binding events to build the kymograph shown in figure 4C (right). As the fluorescence intensity of ATTO647N at the binding step (Fig. 4C, left) and before the photobleaching step (Fig. 4C, middle) are comparable with the ATTO647N signal that did not lead to DNA loop extrusion (Fig. 4C, right), we used $\sim 600 \pm 170$ a.u. fluorescence intensity (from figure 4C, right) as the single fluorophore intensity to quantify the number of condensin acting at the stem of the loop (Fig. 4D). Note that the intensities of the three panels can mutually be compared, since they were taken under similar optical conditions.

Supplementary figures

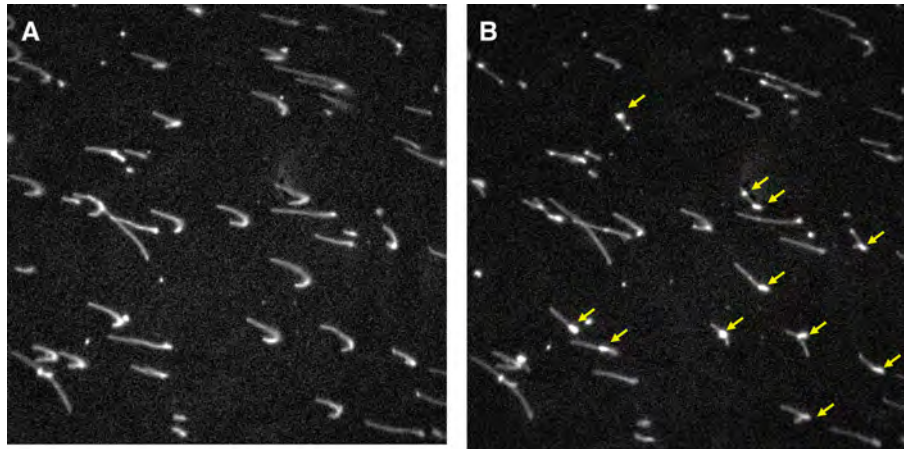


Fig. S1. Example of a field of view showing many SxO-labeled DNA molecules imaged in the presence of flow. This wide-field image shows double-tethered DNA molecules before (A) and after (B) loop extrusion by condensin. Yellow arrows indicate extruded loops.

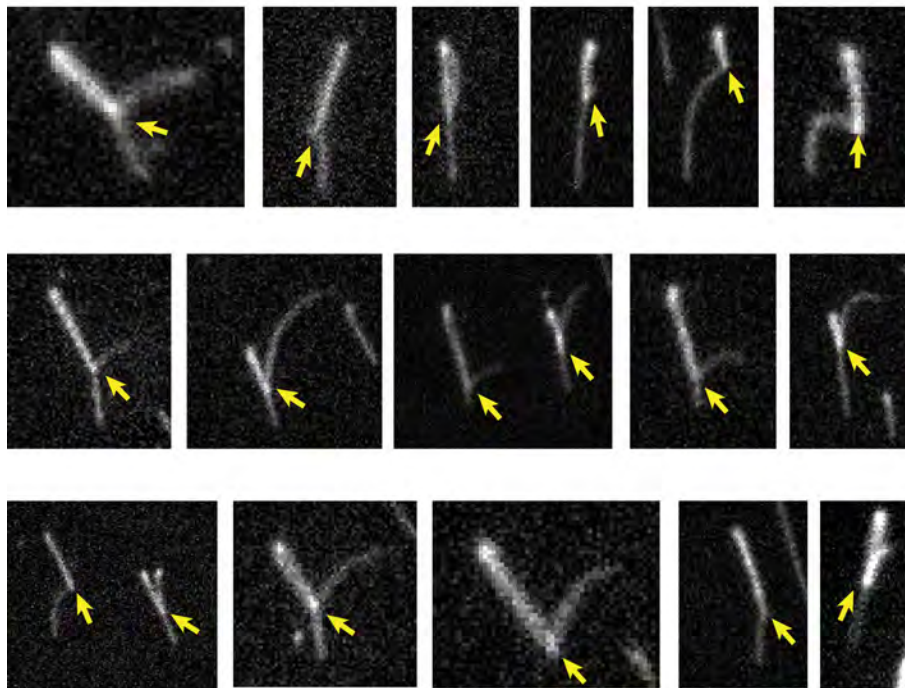


Fig. S2. Visualization of DNA loops that are induced by condensin and visualized by side-pulling through flow stretching. Each panel shows an individual double-tethered DNA molecule that is stained with SxO and that exhibits an extended loop. Yellow arrows indicate the bases of the loops.

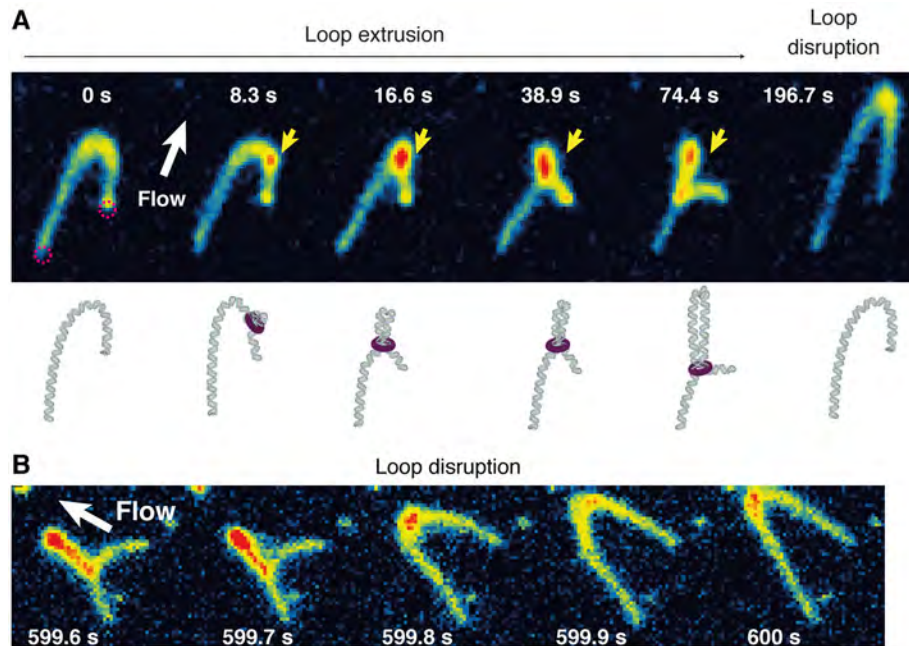


Fig. S3. Real-time loop extrusion and disruption. **(A)** Movie snap-shots showing real-time DNA loop extrusion on double-tethered DNA, which was kept under constant flow. At time 8.3 seconds, a bright fluorescence density appeared (indicated by a yellow arrow), which grew over time until reaching a maximum size at 74.4 seconds. After 196.6 seconds, the loop suddenly disappeared, presumably due to dissociation of the condensin. **(B)** Snapshot images showing the instantaneous disruption of a loop that had been extruded by condensin. These snap-shots are extracted from the same movie as in figure 2A, right before the last snap-shot image shown there.

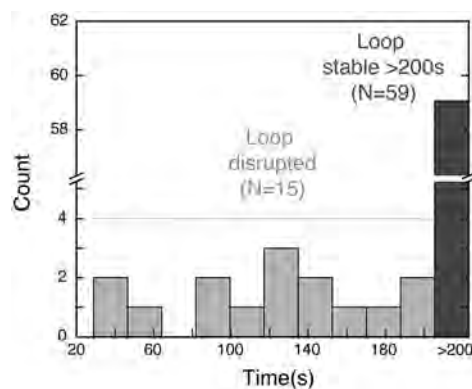


Fig. S4. DNA loops are stable for long periods of time. Plot of the lifetime of extruded DNA loops (defined as the time between their creation and disruption). About 80% of the extruded DNA loops did not release within the observation time of 200 seconds (dark grey bar on the right).

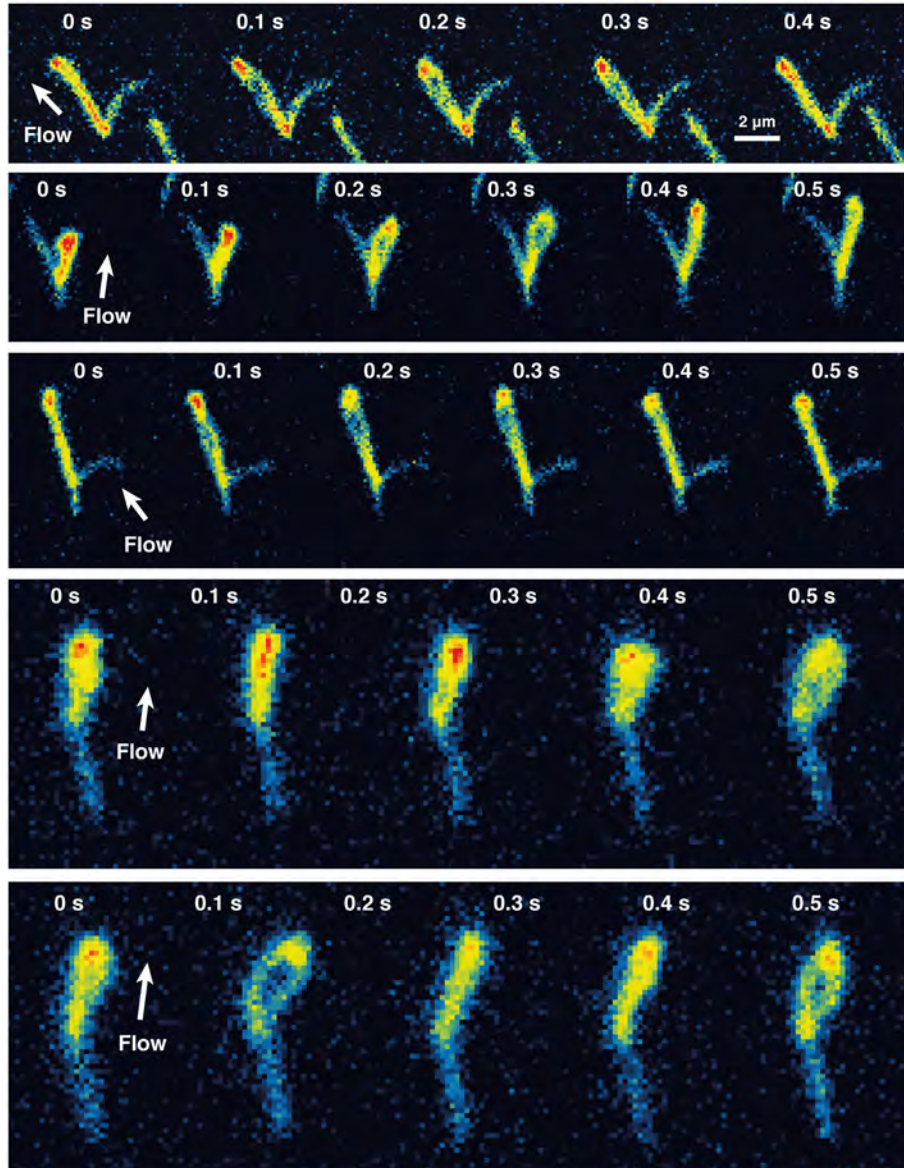


Fig. S5. The extruded DNA is a loop. Series of consecutive images showing spontaneous opening and closing of the DNA loop that was extruded by condensin, similar to data in figure 2B. Each horizontal panel shows a different DNA molecule.

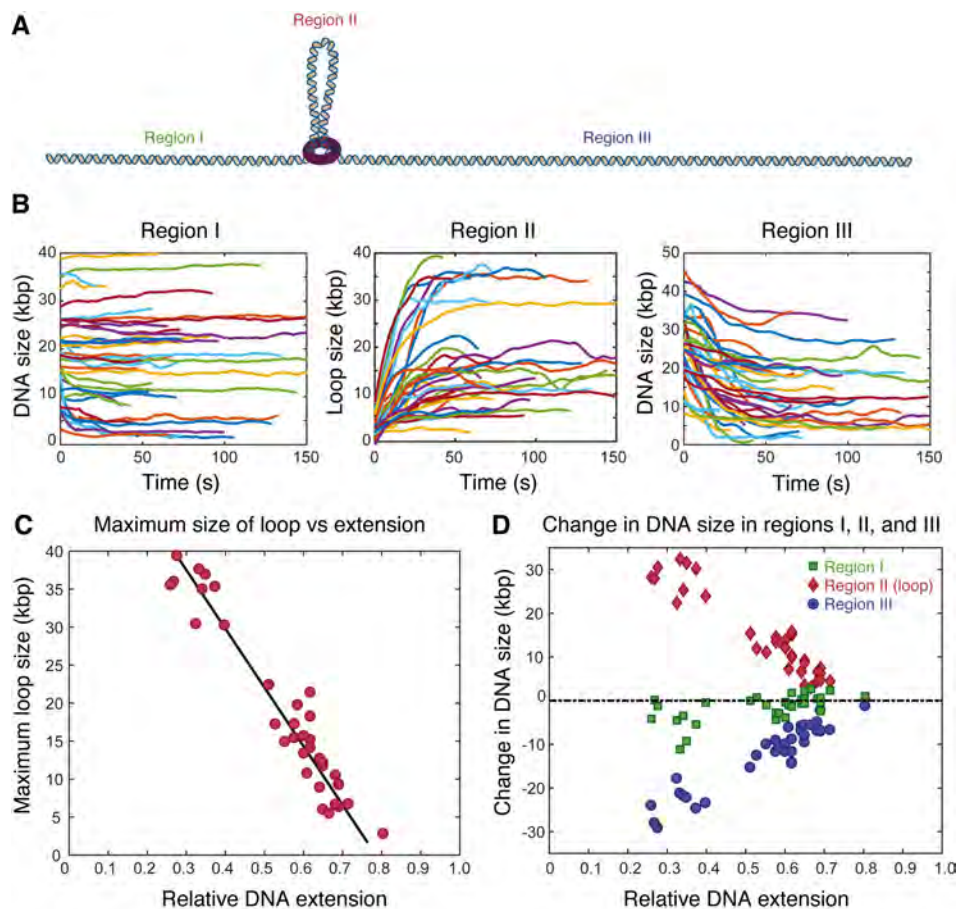


Fig. S6. Loop extrusion is asymmetric. **(A)** Definition of regions I–III. **(B)** Time evolution of DNA length behind (region I), within (II), and ahead of (III) the DNA loop for individual molecules ($N=36$). **(C)** Maximum observed loop size versus relative DNA extension for the data shown in panel (B). The line serves as a guide to eye. Note that the maximum possible loop size in our assay is limited by the 48.5-kbp length of the λ -DNA. **(D)** Size difference for the loop (red), region I (green), and region III (blue) between the start and end of the time traces shown in panel (B), as a function of the relative DNA extension.

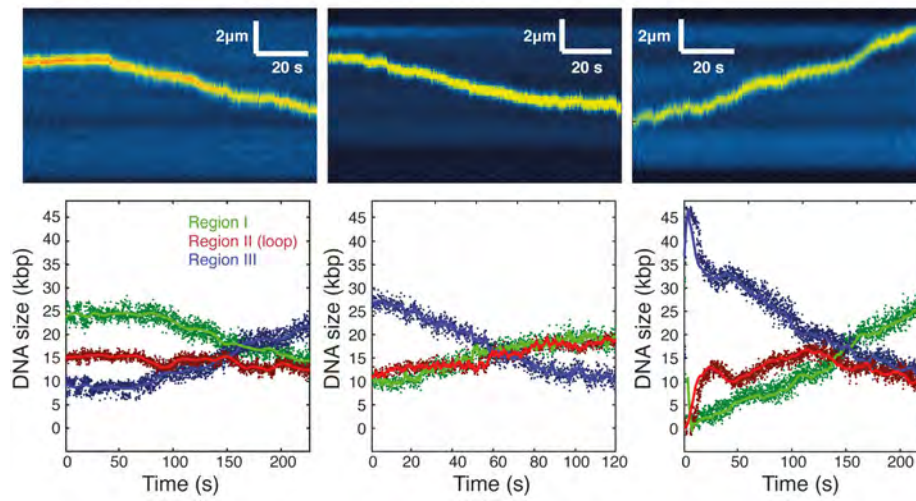


Fig. S7. Three examples of DNA loop dynamics induced by the safety-belt mutant condensin complex. Top row shows kymographs; bottom row shows the time evolution of DNA sizes in regions I, II, and III. The conditions for these data are identical to those of the example shown in figure 3G.

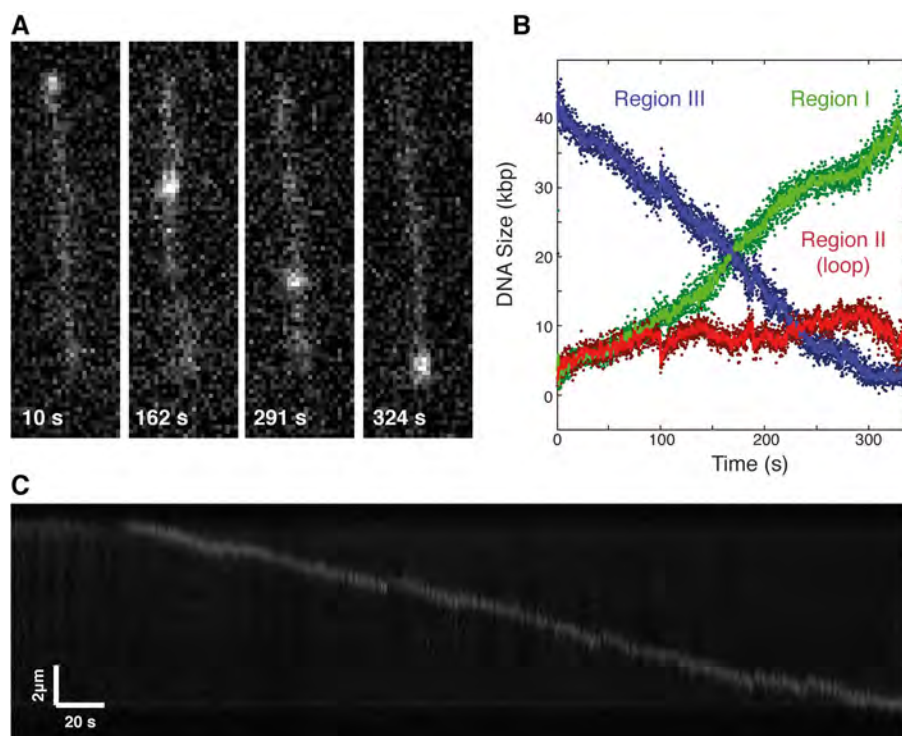


Fig. S8. Visualization of the unidirectional translocation of a DNA loop by the activity of condensin at increased salt concentrations (125 mM NaCl and 10 mM Mg^{2+}). **(A)** Series of snapshot images showing a DNA loop that translocates along the DNA from the top to bottom end with a negligible growth in DNA loop size. **(B)** Corresponding time evolution of DNA size in the regions I, II, and III. Using the slopes in the I and III curves, the loop speed in this example can be estimated to be 112 bp/s, which is of the same order of magnitude as the movement rate of condensin DNA curtains at 63 ± 36 bp/s (mean \pm SD) under identical buffer conditions (12). **(C)** Kymograph of the SxO fluorescence intensities shown in (A).

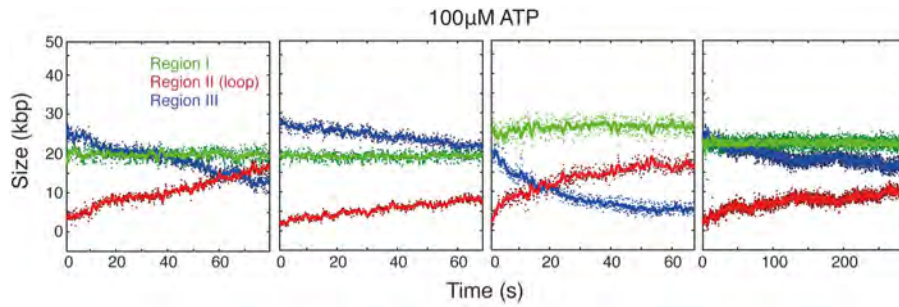


Fig. S9. Four examples of DNA loop extrusion by condensin at a reduced ATP concentration of 100 μM .

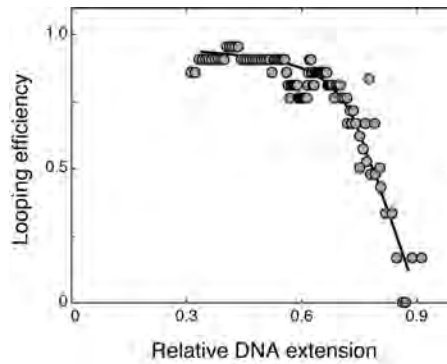


Fig. S10. Loop extrusion efficiency (defined as the number of molecules where a loop is formed within the observation window of 200 seconds, relative to the total number of DNA molecules examined) as a function of relative DNA extension. Each data point was obtained by calculating the fraction of molecules from 20 molecules with a specified mean relative DNA length. The line serves to guide the eye.

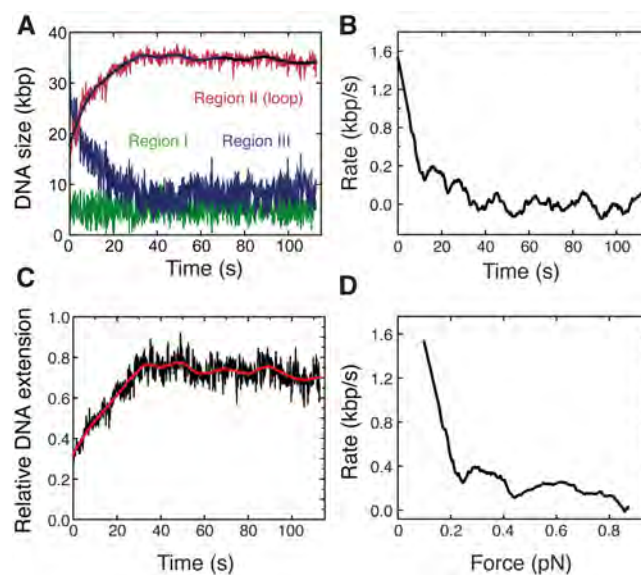


Fig. S11. Example of the extraction of the rate versus force plots. **(A)** The loop size in kbp (region II, red) was first smoothed via Savitzky-Gollay filtering with 2nd order polynomial and 200 points (black line). **(B)** The rate of loop extrusion was then obtained from the first-order derivative of the adjacent points of the smoothed curve. **(C)** To obtain force values, the relative extension of DNA, defined as the end-to-end distance of the molecule divided by the physical length of DNA that is not extruded in the loop (i.e. the lengths of regions III plus I), was extracted and smoothed, followed by conversion to force via linear interpolation of the experimentally obtained force-extension curve (15). **(D)** As a result, the rate of loop extrusion was plotted against the force.

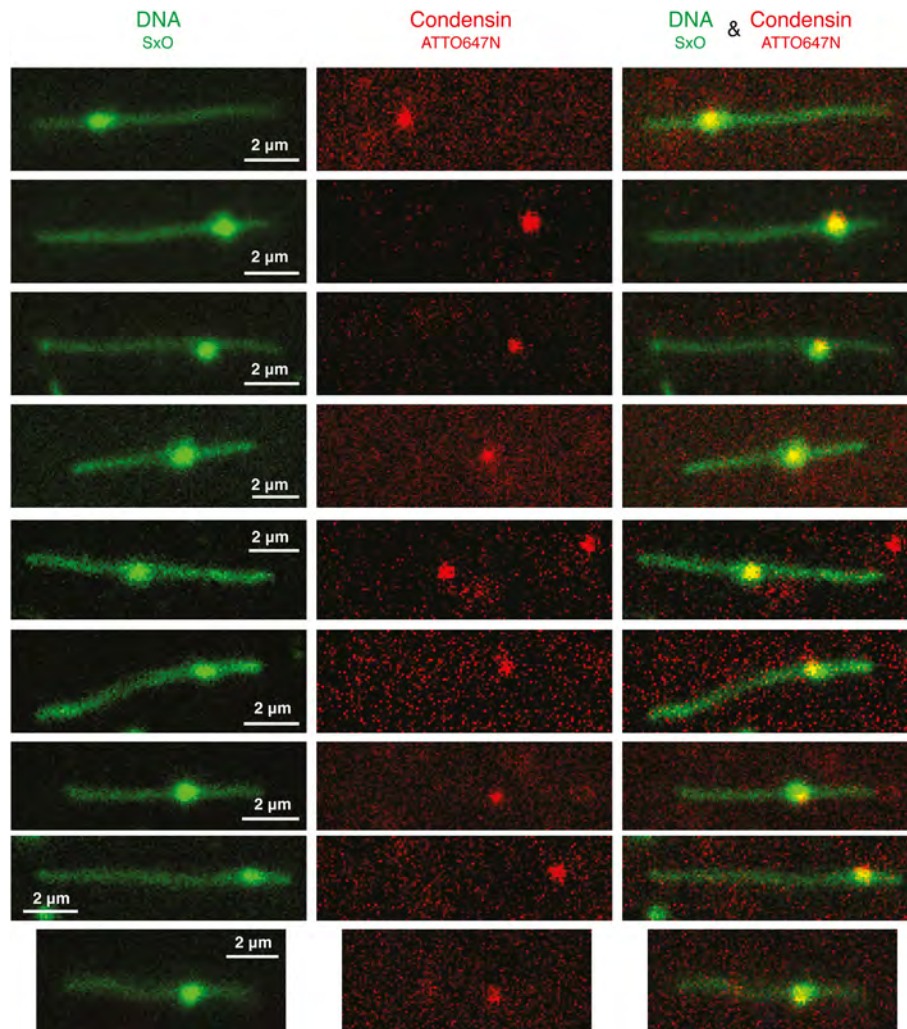


Fig. S13. Co-visualization of a DNA loop and condensin. Fluorescence images of a SxO-stained DNA exhibiting an extruded loop (left panels) and an ATTO647N-labeled condensin located at the stem of the loop (center panels) and merge of both images (right panels). DNA is shown in green and condensin in red.

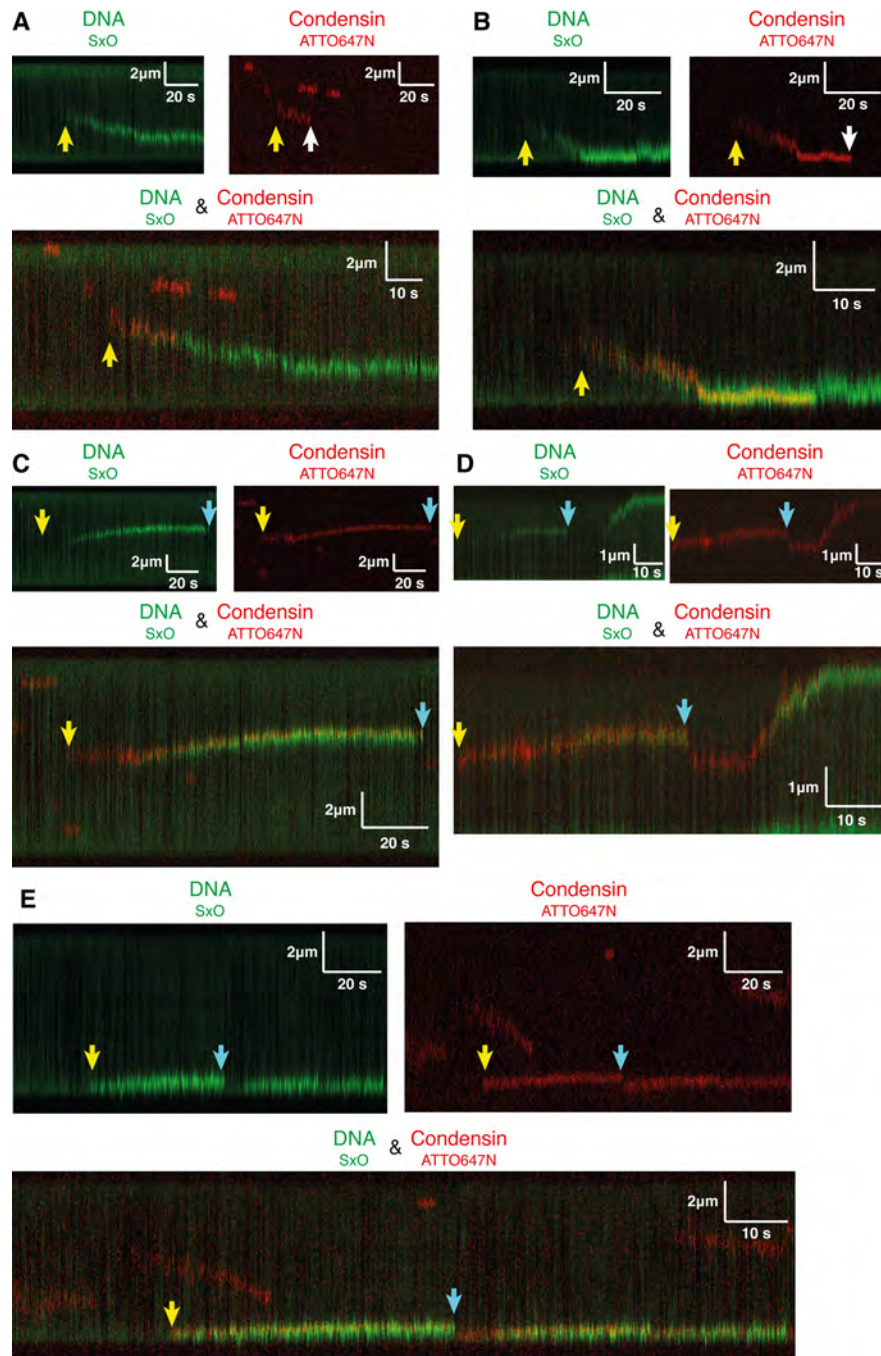


Fig. S14. Additional examples showing DNA loop extrusion by condensin. Kymographs of fluorescence intensities from SxO-stained DNA (green, top left) and ATTO647N-labeled condensin (red, top right) and merge (bottom). Condensin binding is indicated by a yellow arrow. (A–B) Two examples of the single-step disappearance of the ATTO647N fluorescence signal due to photobleaching (white arrow), while the DNA loop remains stable. (C–E) Three examples of the spontaneous disruption of a DNA loop, apparent from the sudden disappearance of accumulated SxO intensity (cyan arrow), while the ATTO647N-condensin signal remains. Subsequently, the bound condensin re-initiated the extrusion of a new DNA loop (D–E).

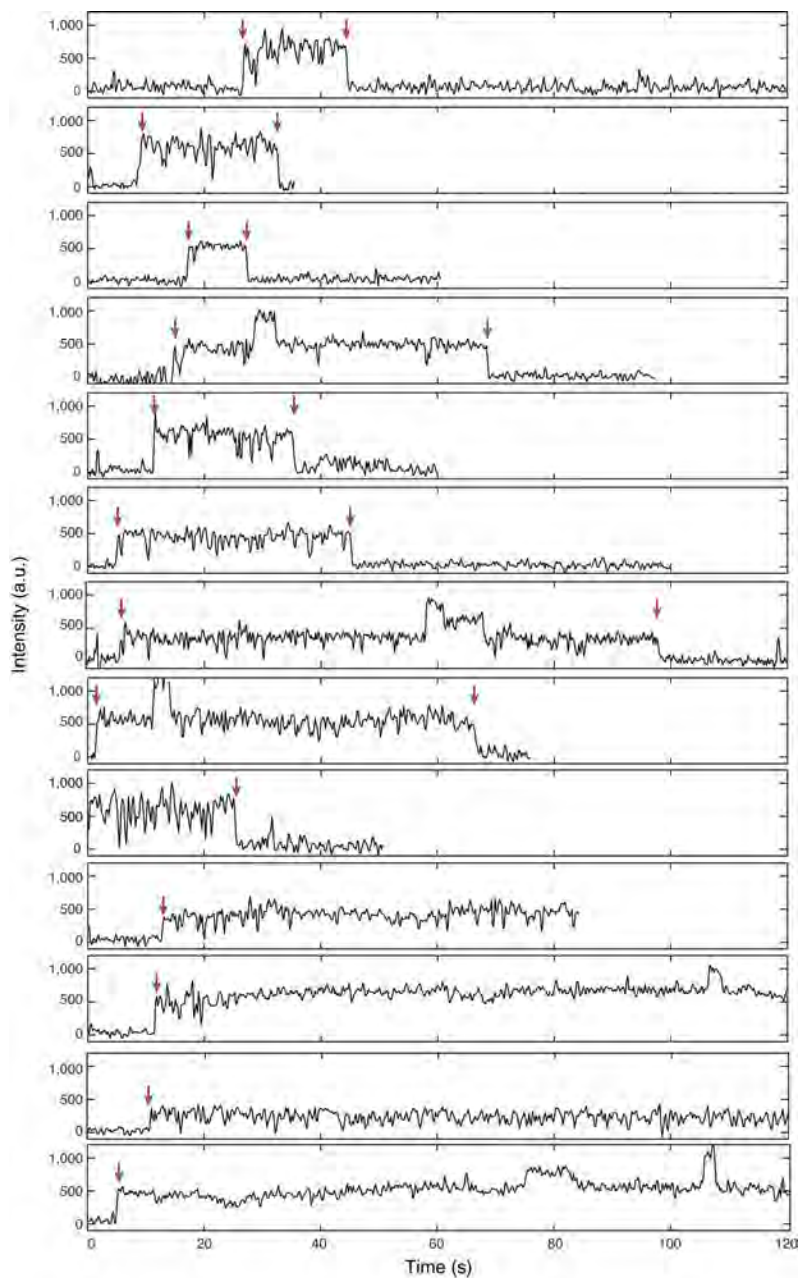


Fig. S15. Time traces of fluorescence intensities of individual ATTO647N-labeled condensin complexes at the stem of DNA loops. The data are obtained from real-time movies showing condensin complexes that bind DNA and induce loop extrusion, sometimes followed by photobleaching of ATTO647N. All binding and photobleaching events occurred as single steps. In the bottom time traces, the ATTO647N signal did not bleach during the 120-s time window displayed. Note that occasionally additional intensity is observed for short periods due to the temporary binding of an additional condensin to the DNA loop. Furthermore, note that the ATTO647N signal intensity of all steps is comparable, further verifying the presence of only a single condensin complex at the stem of the loop.

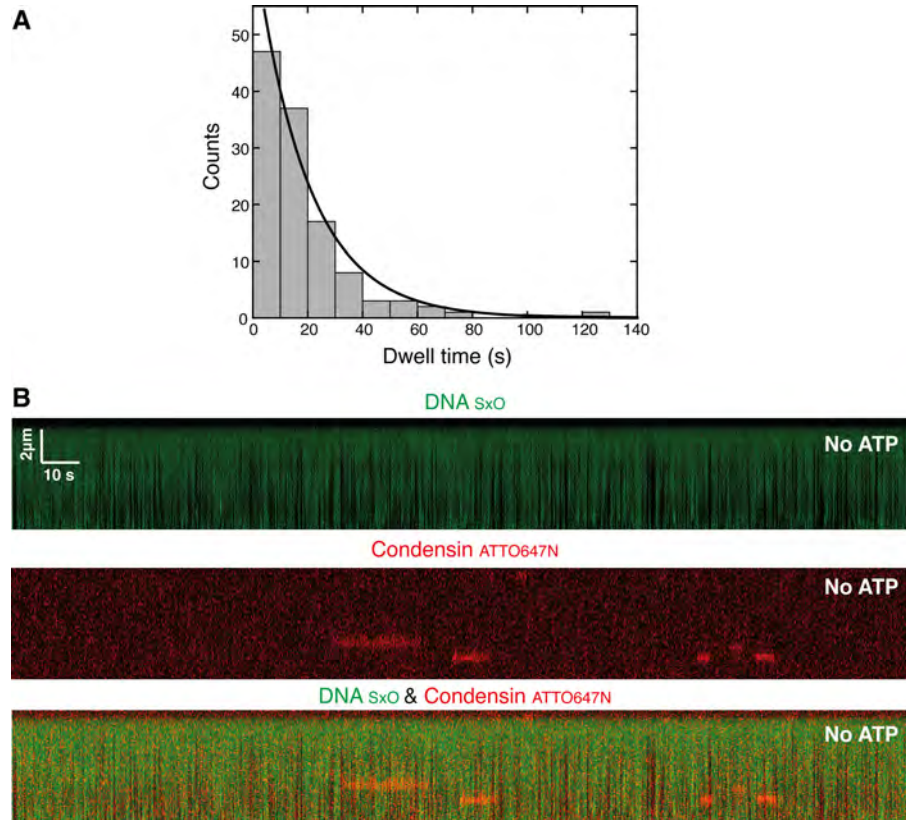


Fig. S16. Condensin binding to DNA without loop extrusion in the absence of ATP. **(A)** Distributions of the dwell times for ATTO647N-labeled condensin that temporarily binds to DNA without resulting in loop extrusion. The solid line shows an exponential decay fit to the data, yielding the mean dwell time of 19 ± 1 seconds. **(B)** Kymograph showing the association and dissociation of ATTO647N-labeled condensin (middle) to DNA (top), without detectible loop extrusion. The merge image is shown at the bottom.

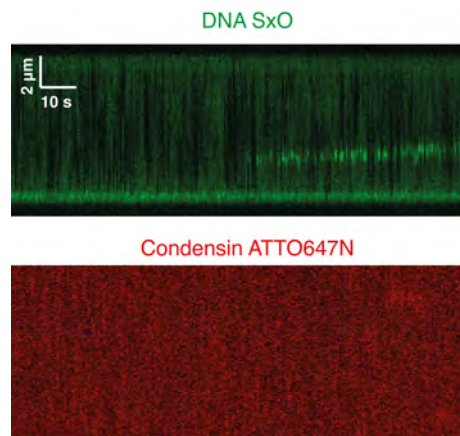


Fig. S17. Example kymograph obtained from the dual-color imaging of SxO-labeled DNA and ATTO647N-labeled condensin, showing DNA loop extrusion without any ATTO647N fluorescence signal in the corresponding channel (presumably due to an unlabeled condensin molecule).

Supplementary movies legends

Movie S1. Movie showing homogenously distributed SxO fluorescence intensity along the length of a double-tethered λ -DNA molecule in the absence of condensin.

Movie S2. Movie showing DNA compaction by condensin. Compaction can be identified as a bright fluorescence spot within the SxO-stained DNA.

Movie S3. Movie showing DNA that has been compacted by condensin. Compaction can be identified as a bright fluorescence spot within the SxO-stained DNA. During this movie, a perpendicular flow is applied to reveal that the bright spot constitutes an extended DNA loop.

Movie S4-S5. Movies showing DNA loop extrusion on SxO-stained DNA under a constant flow. In both movies, DNA initially displays an inverted U shape due to the applied flow. As the movies proceed, a bright fluorescence spot appears that grows into an extended loop, which finally stalls. At its maximum size, the DNA molecule appears as an inverted Y shape.

Movie S6. Movie that shows single-step disruption of the DNA loops at the end of movie S5, resulting in the return of a homogenous DNA intensity that was identical to the bare DNA at the start of the experiment.

Movie S7. Movie showing condensin-mediated DNA compaction under constant flow perpendicular to DNA. Near the end of the movie, the DNA loop splits, most likely due to a photo-induced double strand break. This rare event shows the two DNA strands that form the extruded loop.

Movies S8. Movie of DNA loop extrusion on double-tethered DNA in the absence of flow. The DNA initially exhibits a homogenous fluorescence intensity along its length. As time progresses, a bright fluorescence spot appears that migrates towards one of the two ends of the attached DNA.

Movie S9. Movie with overlaid channels of fluorescence from SxO-stained DNA (green) and ATTO647N-labeled condensin (red), showing condensin localization to the stem of the extruded DNA loop.

Movie S10. Movie with overlaid channels of fluorescence from SxO-stained DNA (green) and ATTO647N-labeled condensin (red), showing the correlative spatial fluctuations of the ATTO647N condensin signal and the SxO DNA loop.

References and Notes

27. J. Yin, A. J. Lin, D. E. Golan, C. T. Walsh, Site-specific protein labeling by Sfp phosphopantetheinyl transferase. *Nature protocols* **1**, 280-205 (2006).
28. J. Yin *et al.*, Genetically encoded short peptide tag for versatile protein labeling by Sfp phosphopantetheinyl transferase. *Proceedings of the National Academy of Sciences of the United States of America* **102**, 15815-15820 (2005).